IEEE Access
Multidisciplinary ⋮ Rapid Review ⋮ Open Access Journal

Received 18 October 2022, accepted 2 November 2022, date of publication 7 November 2022, date of current version 14 November 2022.

Digital Object Identifier 10.1109/ACCESS.2022.3220676

METHODS

An Air Target Course Prediction Method Based on Sub-Regions Divide and Conquer With Double Variable Weight

TONGYAO YANG[1], FENGBAO YANG[1], AND DINGZHU LI[2]
[1]School of Information and Communication Engineering, North University of China, Taiyuan, Shanxi 030051, China
[2]North Automatic Control Technology Institute, Taiyuan, Shanxi 030051, China

Corresponding author: Fengbao Yang (yfengb@163.com)

This work was supported in part by the National Natural Science Foundation of China under Grant 61972363.

ABSTRACT The number and density of airspace decompositions in course prediction are often fixed, resulting in large evaluation errors or low search efficiency of sub-regions, which makes it difficult to take into account the accuracy and real-time performance of course prediction. Aiming at this problem, a model based on the dynamic divide and conquer in sub-regions has been built. Firstly, a new airspace decomposition rule is proposed to adaptively decompose according to the complexity of the environment. Secondly, a state-distance bivariate weight function is constructed. The weights of course prediction index system are dynamically adjusted to improve the evaluation reliability of the selection possibilities of sub-regions. Then, to realize a comprehensive course prediction, the quality function of the course sequence is constructed from length, tortuosity, and selection possibility. Finally, a heuristic function based on possibility factor and distance factor and a pheromone update rule based on positive and negative feedback mechanism are constructed to improve the convergence speed and quality of course prediction. Compared with the airspace uniform decomposition strategy, course evaluation quality function, and ant colony algorithm experiment, the proposed method has a faster convergence speed and a higher sequence quality.

INDEX TERMS Course prediction, direction sequence, dynamic divide and conquer, search algorithm, variable weight theory.

I. INTRODUCTION

With the improvement in anti-jamming and concealment technology [1], it is difficult to obtain the movement state of the enemy target in real time. Therefore, predicting the course of an air target based on the macroscopic situation in advance plays an important role in determining the deployment of air defense forces and seizing battle opportunities [2]. However, the course prediction of aerial targets faces challenges owing to the large combat airspace, high environmental uncertainty, and complex interaction of course influencing factors [3]. The efficient and accurate prediction of the global course of aerial targets in complex environments has become an urgent problem to be solved.

The associate editor coordinating the review of this manuscript and approving it for publication was Zaharias D. Zaharis.

Based on the conceptual model of Situation Awareness (SA) [4] defined from the perspective of people in the ''OODA loop'' of the American psychologist M. Endsley, some scholars regard course prediction of long-term domain as a multi-attribute decision-making problem and divide the direction prediction into three steps. (1) Build a course prediction index system. Song et al. [5] established a course prediction index system for air targets by analyzing situational information, such as terrain, meteorology, electromagnetics, and air defense forces. (2) Decompose the airspace and calculate the index attributes of sub-regions. For example, Ren et al. [6] and Zhu et al. [7] studied the deployment characteristics of an air defense network, and respectively proposed to uniform decomposition of the airspace into fan-shaped or annular regions. (3) The multi-attribute decision-making methods [8], [9], [10], [11] are used to calculate the

possibility of each sub-region, and the sub-regions with the largest possibility are selected as the most likely flight direction. Such as Yang et al. proposed to use the TOPSIS algorithm to analyze the course prediction index values and rank the selection possibilities of each direction [12]. Ma et al. constructed a convolutional neural network and predicted the main selection directions for an air target [13]. At present, scholars focus on building a complete course forecasting index system and studying multi-attribute decision-making methods to improve the reliability of flight selection in sub-regions, but ignore the impact of the airspace decomposition strategy on course prediction. The methods proposed in the aforementioned divide the airspace into fan-shaped or annular regions at equal intervals. The coverage of sub-region is large, not only is the evaluation error of the course prediction indicator large, but also the result is a single-angle range, which provides limited information for combat auxiliary decision-making.

Similar to predicting global course based on multi-attribute decision making, the path planning problem under macro-modality constraints is the optimal choice of accessible sub-region sets [14]. The research idea is to evenly decompose the motion region into a large number of sub-regions [15], [16], and search for the sub-regions set that satisfies the objective function in the passable regions to achieve the optimal path planning. Scholars from various countries focus on improving the search-path time, search-path integrity and search-path optimality, and their research results are mainly divided into heuristic algorithms,(such as A* algorithm [17], D* algorithm [18]) evolutionary algorithms(such as ant colony algorithm [19], particle swarm algorithm [20], genetic algorithm [21]) and potential field algorithms (vector field [22], artificial potential field [23]). Among them, the evolutionary algorithm has the characteristics of self-organization, self-adaptation and self-learning. Compared with PSO, GA and other evolutionary algorithms, ACO is more suitable to solve the problem of searching the path on the graph [24], [25], [26].

Inspired by the research idea of path planning, this study combines the advantages of multi-attribute decision-making and ACO, and proposes an efficient course prediction method based on the dynamic division and conquer of sub-regions. Using the idea of ''dynamic divide and conquer'' to adaptively decompose the airspace, not only can the sub-regions be evaluated from multiple indicators to meet the requirements of flight safety and concealment, but also the decomposition of the sub-regions can dynamically change according to the complexity of the environment, which can meet the requirements of real-time and accurate course prediction. The main contributions of this study are as follows. (1) An adaptive airspace decomposition rule based on the spatial distribution of flight obstruction factors is proposed. (2) The state-distance variable weight function is constructed by analyzing the characteristics of flight direction selection. (3) The quality function of the flight direction is constructed from the sequence length, tortuosity, and selection probability. (4) In addition, a heuristic function based on possibility factor and distance factor and a pheromone update rule based on positive and negative feedback mechanism are constructed, which improves the convergence speed and quality of prediction.

The remainder of this paper is organized as follows. Section 2 briefly introduces the relevant theories, Section 3 introduces the method proposed in this paper. Section 4 shows the simulation experiments and discussion. Section 5 presents the conclusions of this study.

II. RELATED THEORIES

A. VARIABLE WEIGHT THEORY

To a certain extent, the synthesis of constant weights reflects the relative importance order of various indicators and is widely used because of its simplicity and certain rationality. However, regardless of the value of each indicator, the weight vector W remains fixed, which often leads to unreasonable comprehensive results in practical problems, that is, the problem of ''state imbalance''. The idea of variable weight is to dynamically adjust the weight vector, which not only considers the relative importance order of each indicator, but also considers the degree of state balance, thus solving the problem of ''state imbalance'' to a certain extent [27].

In the paper [28], the zoning variable weight function (1) is shown as follows:

$$S_j(p) = \begin{cases} \frac{c_2-c_1}{\lambda-\mu}\mu In\frac{\mu}{p_j} + c_2, & 0 \le p_j \le \mu \\ -\frac{c_2-c_1}{\lambda-\mu}p_j + \frac{c_2-c_1}{\lambda-\mu}, & \mu < p_j \le \lambda \\ C + \frac{c_2-c_1}{2(\lambda-\mu)(\alpha-\lambda)}(\alpha-p_j)^2, & \lambda < p_j \le \alpha \\ C, & \alpha < p_j \le \beta \\ K(1-\beta)In\frac{1-\beta}{1-p_j} + C, & \beta < p_j \le 1 \end{cases} \tag{1}$$

$S_j(p)$ is smooth and continuous on the interval (0,1), $\mu, \lambda, \alpha, \beta$ represent the interval thresholds, $x_i$represents the comment value *i-th* indicator, c_1, c_2, K, C are constants determined by the actual condition. $0 < \mu < \lambda < \alpha < \beta < 1, 0 < C < c_1 < c_2 < 1$. When $\mu = 0.2, \lambda = 0.4, \alpha = 0.7, \beta = 0.9$ and $C = 0.4, c_1 = 0.6, c_2 = 0.8$, the function $S_j(p)$ is shown in Fig.1.

The variable weight vector can be expressed as the normalized product of the constant weight vector and the state variable weight vector, and the calculation formula is as follows:

$$w_j^p(x_1, \cdots x_m) = \frac{w_j^{(0)} S_j(p_1, \cdots, p_m)}{\sum_{j=1}^{m} w_j^{(0)} S_j(p_1, \cdots, p_m)} \tag{2}$$

B. ANT COLONY OPTIMIZATION

Ant colony optimization (ACO) is a bionic algorithm proposed by Italian Dorigo et.al according to the law of the overall foraging behavior of the ant colony [29]: the individuals in the ant colony will leave a chemical substance

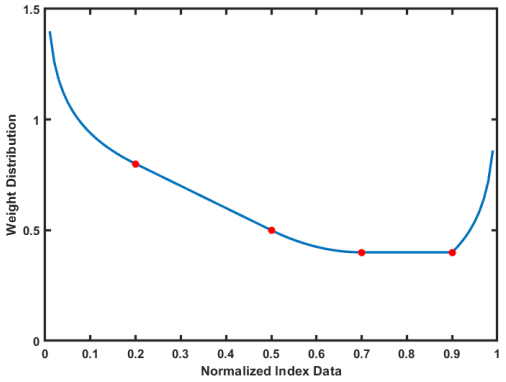

FIGURE 1. Variable weight function based on state value.

called ''pheromone'' on the walking path, and update the pheromone [30] on each path as shown in Eq.(3):

$$\tau_{KP}(t+n) = (1-\rho) \times \tau_{KP}(t) + \tau_{KP}(t) \tag{3}$$

where $\rho \in (0, 1)$ is the global pheromone volatilization coefficient. $\tau_{KP}(t)$ is the positive change of the pheromone on the path KP in the current iteration, as shown in Eq.(4):

$$\tau_{KP}(t) = \sum_{A=1}^{m} \tau_{KP}^{A}(t) \tag{4}$$

where $\tau_{KP}^{A}(t)$ is the concentration of left pheromones by ant A on path KP. If ant A has not passed the path KP, the value is 0.

And other individuals have a keen perception of this ''pheromone'', in the face of different paths, they will actively choose the path with more ''pheromone'', and leave the same ''pheromone'' on the path, which will lead to the ''pheromone'' on a certain path more concentrated. Under the premise that ''pheromones'' continue to grow positively, the colony will gradually determine the optimal path, so as to quickly find food [31].

$$P_K^A = \begin{cases} \dfrac{\tau_K\,(t)^{\alpha}\,\xi_{KP}\,(t)^{\beta}}{\sum\limits_{c \in allowA} \tau_K\,(t)^{\alpha}\,\xi_{Kc}\,(t)^{\beta}}, & c \in allow\ A \\ 0, & c \notin allow\ A \end{cases} \tag{5}$$

where ξ is the heuristic information, $\xi_{KP}\,(t)^{\beta}$ represents the degree of transition expectation of ant A from node K to node P, α is the pheromone concentration factor. β is the expected heuristic factor. After ant A completes one iteration, the route taken from the starting node to the target node is a feasible solution.

Ant colony algorithm is constructed by pheromone positive feedback effect and heuristic function, and has strong robustness and adaptability.

III. METHOD

In view of the large airspace coverage and many factors affecting the flight direction of the air target, it is difficult to accurately evaluate the course prediction index of the entire airspace, which affects the prediction accuracy. The main idea of the divide-conquer strategy is to divide a large problem that is difficult to solve directly into some smaller-scale problems, so as to conquer them down one by one [32]. The decomposition of the problem and the combination of the decompositions have a significant impact on the quality and efficiency of solving complex problems. Therefore, based on the uncertain distribution of influencing factors in the airspace and the demand of air target flight selection, this paper proposes an efficient prediction method of flight direction based on a dynamic divide and conquer strategy. The flow chart is shown in Fig.2, which is divided into the following three steps. (1) Airspace is adaptively decomposed based on the spatial distribution of flight obstruction factors. (2) The weights of the course prediction indicators are dynamically adjusted according to the indicator state value and flight distance, and the selection possibility of sub-regions from multiple indicators can be calculated. (3) Construct a course quality assessment function, and search for the sub-region set based on the improved ant colony algorithm. Course sequence prediction of air targets is realized. These three steps are described in detail in Section III.A,B,C.

A. DIVIDE: ADAPTIVE DECOMPOSITION RULES

The reasonable decomposition of airspace has an important impact on the accuracy and real-time performance of direction prediction. When the number of sub-regions in the airspace is too small, the coverage of sub-region is large, and the accuracy of the prediction results is low. When the number is too large, it is easy to cause poor real-time prediction performance owing to the wide search range. Therefore, an adaptive spatial decomposition rule based on distribution of flight obstruction factors is proposed. The number and density of sub-regions can change with the complexity of the airspace environment, which can improve the accuracy of evaluations and search efficiency in sub-regions and is of great significance for timely and accurate direction prediction. The specific steps are as follows.

(1) First-level decomposition. Obstructive factors refer to those related to the flight safety of air targets, making it necessary to change the direction, such as regions with dense strong storms. The airspace from the flight start point to the end point is divided into different ring layers according to the spatial distribution information of obstacles. When the number of obstacles is large and the distribution of obstacles is relatively discrete, the number of divided ring layers is large. Conversely, the number of divided ring layers is small. As shown in Fig.3 (a), E is the starting position of the air target, T is the ending position, and $o1$, $o2$, and $o3$ are the three flight obstacles in the flight airspace. Taking the flight end point as the center, the distances between the three obstacles and the flight end point are calculated, and the flight airspace is divided into four ring layers with distances as the radius.

(2) Second -level decomposition. Because the distribution of the obstacles in the outer layer is often discrete, to reduce the large evaluation error of the sub-regions, the ring layers

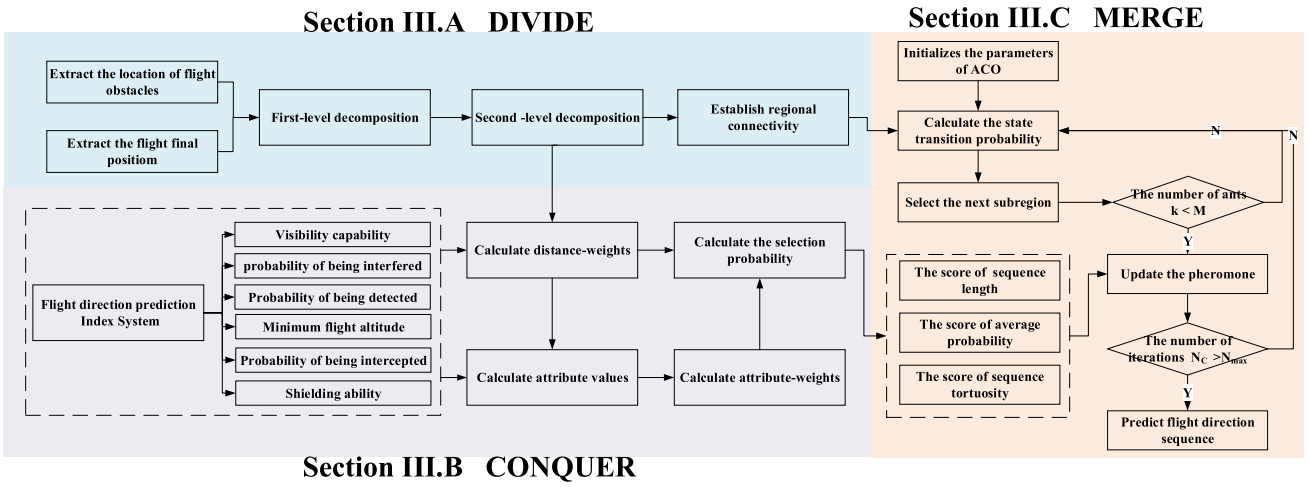

FIGURE 2. Flow chart of course prediction based on sub-regions divide and conquer.

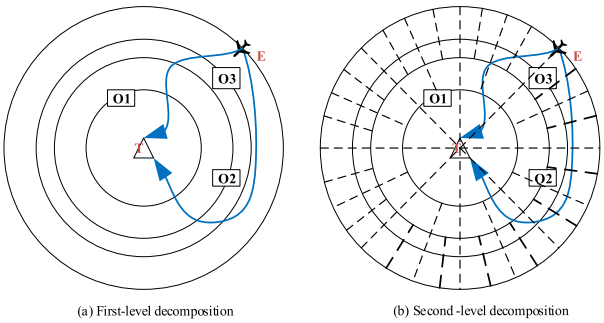

FIGURE 3. Adaptive spatial decomposition rules.

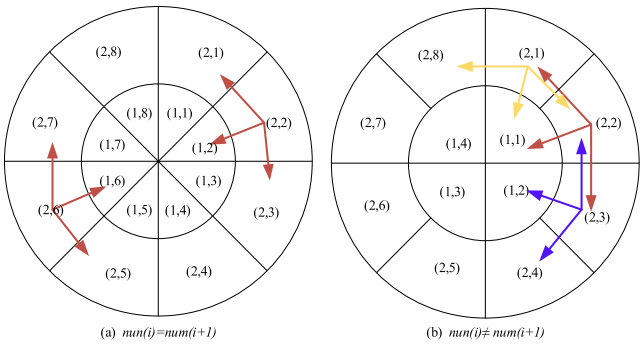

FIGURE 4. Connectivity relationship of sub-regions.

are divided into 32, 16 and 8 sub-regions from the outside to the inside in this paper. As shown in Fig.3 (b), the first ring layer ($o1$-T) is divided into 8 sub-regions, the second ring layer ($o2$-$o1$) is divided into 16 sub-regions, the third ring layer ($o3$-$o2$) and fourth ring layer (E-$o3$) are divided into 32 sub-regions.

Simultaneously, the connectivity relationship between sub-regions has the following definitions:

a) There are two ways to describe subregions: *region* (i, j) represents the relative position between sub-regions, that is, the current sub-region is located in the j-*th* discrete region of the i-*th* ring layer. i and j are the corresponding results of the first-level and second-level decompositions. $\left(x_{(i,j)}, y_{(i,j)}\right)$ represents the relative position in the airspace, x represents the distance from the flight end point in the x axis, and y represents the distance from the flight end point in the y axis.

b) There is no connectivity between the innermost sub-regions. The ring layers are unidirectionally connected. They can only be connected from the outer ring to the inner ring and cannot be connected in the reverse direction.

c) There are only three choices from the current sub-region to the next sub-region. The connectivity of sub-regions is shown in Fig.4. If the numbers of sub-regions of two adjacent layers are same, the next possible sub-region are shown in Fig.4 (a). But if the numbers of sub-regions of two adjacent layers are different, the next optional sub-regions are shown in Fig.4 (b). Therefore, there is the following mathematical description:

$$next = \begin{cases} [(i+1, j-1), (i+1, j+1), (i, j)], \\ \quad if\ num(i) = num(i+1) \\ [(i+1, j-1), (i+1, j+1), (i, \lceil j/2 \rceil)], \\ \quad if\ num(i) \neq num(i+1) \end{cases} \tag{6}$$

where $num(L_i)$ and $num(L_{i+1})$ are the total numbers of sub-regions in L_i and L_{i+1} layer respectively. $\lceil n/2 \rceil$ is a ceiling operation.

B. CONQUER: CALCULATION SELECTION PROBABILITY OF SUB-REGION

1) STATE-DISTANCE VARIABLE WEIGHT FUNCTION

There are many factors that affect flight direction of air target. We calculate the probability of flight selection in each region based on the six indicators in this paper [33]. Visibility capability P_1, probability of being interfered P_2, probability of being detected P_3, minimum flight altitude P_4, probability of being intercepted P_5, shielding capability P_6. The

weight of the course prediction index system is not only related to the state value, but also closely related to the flight distance. For example, in the initial stage of the flight, the air target pays more attention to the flight concealment when choosing the direction, and in the final flight stage, it pays more attention to the survivability. Therefore, it is necessary to analyze the change in the weights of the course prediction index with the flight distance and construct the distance variable weight function.

Let the weight $w_j^d(d_1, \cdots d_m)$ be a function of the flying distance vector $D = (d_1, \cdots, d_m)$. $w_j^d(d_1, \cdots d_m)$ is similar to the state variable weight and also meets the requirements of normality, continuity and hybrid property.

(1) Normality: $\sum_{\mathrm{j}=1}^{m} w_j^d(D) = 1$.

(2) Continuity: $w_j^d(D), \mathrm{j} = 1, 2, \cdots, m$ is on the continuous of independent variables.

(3) Hybrid property: $w_j^d(d_1, \cdots, d_o), o < m$ is monotonically decreasing (increasing), $w_j^d(d_{0+1}, \cdots, d_m)$ is monotonically increasing(decreasing).

According to the characteristic that the weights of course prediction index changes with flight distance, the distance variable weight function is divided into four intervals in this paper, and the zonal hybrid distance variable weight vector function is constructed as shown in Eq.(7). When the distance is $0 \le d_j/D \le d_1$, $S(d)$ is a linear function, which presents an "incentive" state to the weight, and the growth trend is fixed. When the distance is $d_1 < d_j/D \le d_2$, $S(d)$ is an exponential function, the weight is in the state of "strong incentive", and the "incentive degree" shows an increasing trend. When the flight distance is $d_2 < d_j/D \le d_3$, $S(d)$ is a sin function, which is "punishment" to the weight, and its penalty intensity is also changing. When the distance reaches $d_3 < d_j/D \le 1$, the "punishment" of the distance weight function will be zero, and the $S(d)$ will tend to a stable value k_3.

$$S_j(d) = \begin{cases} \dfrac{k_1 - k_0}{d_1}\dfrac{d_j}{D} + k_0, \\ \quad 0 \le \dfrac{d_j}{D} \le d_1 \\ \dfrac{k_1 - k_0}{d_1}\left(\exp\left(m\left(\dfrac{d_j}{D} - d_1\right)\right) - 1\right) + k_1, \\ \quad d_1 < \dfrac{d_j}{D} \le d_2 \\ \dfrac{k_2 - k_3}{2}\sin\left(\dfrac{d_j/D - d_2}{d_3 - d_2}\pi + \dfrac{\pi}{2}\right) + \dfrac{k_2 + k_3}{2}, \\ \quad d_2 < \dfrac{d_j}{D} \le d_3 \\ k_3, \quad d_3 < \dfrac{d_j}{D} \le 1 \end{cases} \tag{7}$$

where d_j represents the distance between the current position and the flight start point, D represents the distance between the start point and the end point, and d_j/D is the normalized distance value. $0 \le d_1 \le d_2 \le d_3 \le 1$ are the distance threshold values of the four intervals, and k_0, k_1, k_2, k_3 are the distance "incentive" or "punishment" values of the corresponding interval.

The corresponding distance weight is calculated as shown in Eq.(8):

$$w_j^d(d_1, \cdots, d_m) = \frac{w_{\mathrm{j}}^{(0)} S_j(d_1, \cdots, d_m)}{\sum_{j=1}^{m} w_{\mathrm{j}}^{(0)} S_j(d_1, \cdots, d_m)} \tag{8}$$

The minimum flight altitude P_4 measures the passable state of the air target, and its importance does not change with flight distance, but its relative weight changes with other indicators. Visibility capability P_1 determines the ability to acquire situation information, which occupies a large weight in the whole flight process and the degree of change is not large. In the initial stage of flight, the air target should ensure concealment of flight as much as possible, the weight of shielding capability P_6 is relatively high, the weight of the probability of being interfered P_2 and the probability of being intercepted P_5 are relatively low. Compared with the initial stage, in the second stage of flight, the weights of P_2 and P_5 are also increased to varying degrees. And in order to gain the time advantage, increasing the weight of the probability of being detected P_3 to avoid being discovered by the detector. In the final flight process, in order to ensure the effect of mission execution, the weights of P_2 and P_5 are relatively high, and the growth rates are faster, but the weight of P_6 is relatively small.

Based on the above analysis, this paper sets the parameters in $S(d)$ of $P_1 - P_6$, as shown in Fig.5(a). The relative distance weights of $P_1 - P_6$ are shown in Fig.5(b).

In this paper, based on the classical sum-type equilibrium function, a state-distance double variable weight function is constructed, and its corresponding comprehensive variable weight model is shown in Eq.(9):

$$\begin{aligned} &w_j^*(x_1, \cdots x_m; d_1, \cdots d_m) \\ &\quad = \frac{w_{\mathrm{j}}^{(0)} S_j(x_1, \cdots x_m) S_j(d_1, \cdots d_m)}{\sum_{j=1}^{m} w_{\mathrm{j}}^{(0)} S_j(x_1, \cdots x_m) S_j(d_1, \cdots d_m)} \end{aligned} \tag{9}$$

where $w_j^{(0)}$ is the initial weight of the *j-th* index.

P_1, P_4, P_6 are benefit-type indicators, the greater the value, the greater the possibility of selecting the sub-region. P_2, P_3, P_5 are cost-type indicators, and the smaller the value, the greater the possibility of selecting the sub-region. Therefore, it is necessary to preprocess the index values when calculating the state weight: $\dot{P}_2 = 1 - P_2, \dot{P}_3 = 1 - P_3, \dot{P}_5 = 1 - P_5$.

The selection probability of sub-region is calculated as shown in Eq.(10):

$$P_{cs} = w_1^* P_1 + w_2^* \dot{P}_2 + w_3^* \dot{P}_3 + w_4^* P_4 + w_5^* \dot{P}_5 + w_6^* P_6 \tag{10}$$

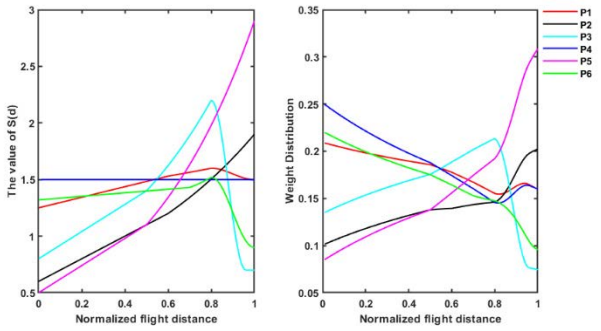

(a) $S(d)$ of $P_1 - P_6$ (b) The relative distance weights of $P_1 - P_6$

FIGURE 5. Variable weight function based distance.

2) EFFECTIVENESS ANALYSIS OF DOUBLE VARIABLE WEIGHT

The normalized distance is respectively $dis = [0.1, 0.3, 0.5, 0.7, 0.9]$. Set the pre-processed state values of course prediction indicators as follows:

	P_1	$\dot{P}_2$	$\dot{P}_3$	P_4	$\dot{P}_5$	P_6
S_1	0.5	0.5	0.5	0.5	0.1	0.5
S_2	0.5	0.5	0.5	0.5	0.3	0.5
S_3	0.5	0.5	0.5	0.5	0.5	0.5
S_4	0.5	0.5	0.5	0.5	0.7	0.5
S_5	0.5	0.5	0.5	0.5	0.9	0.5.

The distance variable weight function Eq.(8) and the state-distance double variable weight function Eq.(9) are used to calculate the course index weights. And the selection possibility is calculated under different index state values at different distances according to Eq.(10). The calculation results are shown in the Fig.6. Although there are some differences between the possibilities in the two cases, the change trend of possibility is the same.

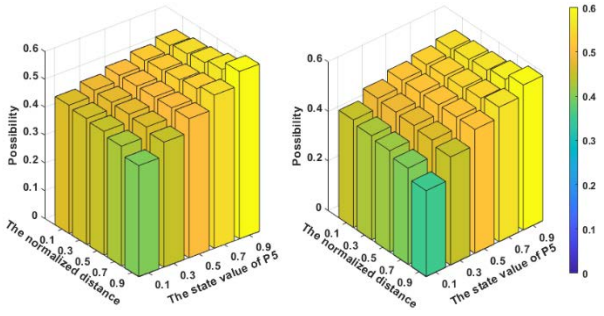

(a)Selection possibility based on distance variable weight (b) Selection possibility based on state-distance variable weight

FIGURE 6. Selection possibility based on different variable weight functions.

According to the selection possibility in Fig.6, the average selection possibilities of two variable weight functions at different normalized distances under the same course index value are shown in Fig.7(a). The change trend of the selection probabilities under the two variable weight functions is the same as that under the state variable weight, which is consistent with the fact that the more favorable the state value, the higher the selection probability. However, when the selection probability is calculated based on the distance variable weight function, the maximum difference value of the average probability under different states is 0.125, and the phenomenon of "state imbalance" still exists. The maximum difference values in the average probability based on the state variable weight and the state-distance variable weight are 0.1628, 0.1522.

According to the selection possibility in Fig.6, calculate the standard deviation of the possibilities with two variable weight functions at different state values under the same normalized distance. As shown in Fig.7(b), basedonly on the state variable weight function, the selection possibility does not change with distance, and the standard deviation is 0. However, based on the state-distance double variable weight, the possibility of lower state values is lower, and the possibility of higher state values is higher, which highlights the difference in the selection possibility caused by the change in state values. Especially when $dis = 0.7$ and $dis = 0.9$, the standard deviations increase by 0.0115 and 0.0138 respectively compared with those based on the distance variable weight.

Based on the above analysis, the state-distance variable weight function proposed in this paper can combine the characteristics of course index weight changing with flight distance, and the advantages of the state variable weight to reduce the "state imbalance", and improve the rationality of course prediction weight allocation. Therefore, the proposed double variable weight function is adopted in the simulation experiment in Section 4.

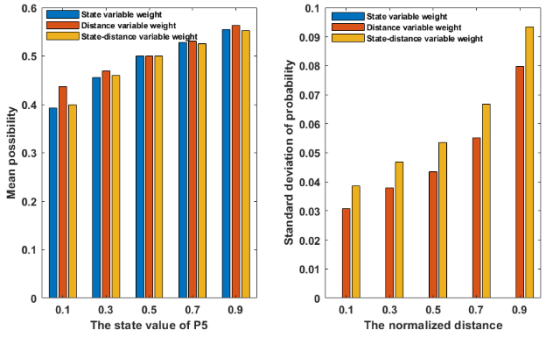

(a) Average selection probability under different state values (b) Standard deviation of selection probability under different distances

FIGURE 7. Distribution of selection probability under different weight functions.

C. MERGE: SEARCHING FOR A SET OF SUB-REGIONS

The set of sub-regions with greater possibility is often selected as the flight direction. Owing to the limitations of flight performance, the quality function of course sequence is constructed from length, tortuosity and selection possibility. ACO has shown good performance in searching the path on the graph, such as strong robustness, distributed computing,

and ease of combination with other methods. Its positive information feedback mechanism enables it to find better solutions quickly [34]. However, when the flight environment is complex, the ant colony has a large search space when selecting the next region, and it takes a long time to provide positive feedback, resulting in poor real-time performance. And the solution speed of ACO needs to meet the real-time requirements of situational awareness. Therefore, an improved heuristic function and improved pheromone updating rules of ACO are constructed to improve the speed and quality of the solution.

Algorithm 1 Searching for a Set of Sub-Regions

1: Obtain sub area location information and select possibility;
2: Initialize the number of ants M, maximum iteration number $N_{\max}$, weights α, β, ρ, Q, initial sub-region S, flight end T;
3: FOR N=1 to $N_{\max}$ do
4: Put all ants into S;
5: While ant k does not reach T do
6: allowed$_k$ ←the set of reachable region for k
7: Choose the next sub-region by Equation(5)
8: End while
9: If ants have reached T then
10: Calculate the quality evaluation value of course sequence J_k by Equations (11)-(15)
11: J_{best} ← the best course sequence in this iteration;
12: update pheromone on all effective course sequence by Equations (19), (20);
13: else if ants have not reached T then
14: update pheromone on all unreachable course sequences by Equation (18);
15: end if
16: end for
17: Output the optimal subregion set

1) QUALITY FUNCTION OF COURSE SEQUENCE QUALITY

The course of air target is described by selecting the sub-region sequence set: $course = \{region_1, \cdots, region_N\}$. The course sequence quality of the feasible solution is evaluated based on three aspects: sequence length, possibility and sequence tortuosity. The length of course sequence is not only limited by the flight range of air target, but also the shorter the sequence length, the shorter the flight time, which has an important impact on the completion of the flight task. The higher the mean probability of the sequence, the lower the risk. In addition, because of the limitations of flight maneuverability, the tortuosity of the sequence should be as smooth as possible. We propose evaluating the direction sequence quality according to Eq.(11).

$$J_{\text{course}} = w_{P_L} P_L(\text{course}) + w_{P_{CS}} P_{cs}(\text{course}) + w_{P_\theta} P_\theta(\text{course}) \tag{11}$$

where $P_L(course), P_{cs}(course), P_\theta(course) \in (0, 1)$ represent the length ratio, mean probability, tortuosity of sequence respectively. The convergence speed of IACO can be improved by unifying each index to [0,1]. The calculation formulas are given in Eq.(12) -Eq.(14). And $w_{P_L}, w_{P_{cs}}, w_{P_\theta}$ are the corresponding weights.

$$P_L(course) = \frac{L_{\max} - L_{course}}{L_{\max} - L_{\min}} \tag{12}$$

where L_{course} represents the total length of the sequence sets: $L_{course} = \sum_{reg=1}^{N-1} \sqrt{\left(x_{reg} - x_{reg+1}\right)^2 + \left(y_{reg} - y_{reg+1}\right)^2}$. $L_{\min}$ is the straight-line distance from the flight start point to the end point. $L_{\max} = L_{\min} + 2\pi L_{\min}$.

$$P_{cs}(course) = \frac{CS_{course}}{N} \tag{13}$$

where CS_{course} represents total probability of sequence sets: $CS_{course} = \sum_{reg}^{N} P_{cs}\,(reg)$. N is the number of sub-regions in the course sequence set.

$$P_\theta(course) = \frac{\theta_{\max} - \theta_{course}}{\theta_{\max}} \tag{14}$$

where $\theta_{\max}$ is a constant that represents the maximum allowable direction tortuosity of the air target. θ_{course} is the cumulative tortuosity of the sub-region sequence, as shown in Eq.(15).

$$\theta_{course} = \sum_{reg=2}^{N-1} \left| \text{atan}\left(\frac{y_{reg+1} - y_{reg}}{x_{reg+1} - x_{reg}}\right) - \text{atan}\left(\frac{y_{reg} - y_{reg-1}}{x_{reg} - x_{reg-1}}\right) \right| \cdot \frac{180}{\pi} \tag{15}$$

The quality value of course sequence is taken as the judgment basis of course prediction accuracy. The higher the quality value of course sequence, the closer the predicted course is to the actual course.

2) CONSTRUCTION OF NEW HEURISTIC FUNCTION

The heuristic factor is the key factor inspiring ants to select nodes, which can directly affect solution quality. When selecting sub-regions, only the selection possibility of sub-region is considered in the heuristic information, which will lead to slow convergence speed and long flight path. Therefore, in order to improve the search efficiency, the influence of the distance between the position of the sub-region and the flight end point is added to the heuristic function, thereby the convergence speed of the algorithm is improved.

$$\eta_{ij} = \left(w_1 P_{cs_{ij}} + w_2 P_{d_{ij}}\right) \tag{16}$$

where η_{ij} is the new heuristic function based on possibility factor and distance factor. $P_{CS_{ij}}$ is the selection possibility of sub-region (i, j), and $P_{d_{ij}}$ is the distance between the center of the sub-region (i, j) and the flight end point, $P_{cs_{ij}}, P_{d_{ij}} \in (0, 1)$, w_1 and w_2 are weights of two heuristic

factors, and $w_1 + w_2 = 1$. The calculation of $P_{d_{ij}}$ is shown in Eq.(17).

$$P_{d_{ij}} = \frac{L_{\min} - d_{ij}}{L_{\min} + \delta} \tag{17}$$

When the flight start point and end point are known, $L_{\min}$ is constant, and $d_{ij} = \sqrt{(x_{ij} - x_{end})^2 + (y_{ij} - y_{end})^2}$ represents the distance between the selected sub-region and flight end point. According to Eq.(17), the closer the last selected sub-region is to the flight end point, the greater the selection probability of sub-region, which reduces the search range and improves the convergence speed.

3) CONSTRUCTION OF NEW PHEROMONE UPDATING RULES

To solve the problem that the global pheromone update rule of ACO cannot guide the ants to search for the optimal solution in time [25], the pheromone update rule based on positive and negative feedback is constructed. (1) The pheromone update rule for the ants trapped in deadlock is shown in Eq.(18). According to the distance between the last selected sub-region and flight end point, the pheromone concentration of selected sub- regions is weakened in different degrees, so as to avoid the blind update of the global pheromone. (2) The pheromone update rule for the ants searched for feasible solutions (from the flight start point to the flight end point) are shown in Eq.(19) and Eq.(20). The increase of pheromone of selected sub-region is not only affected by itself, but also by the optimal course sequence of the current iteration, which effectively improves the convergence speed and search quality of the algorithm.

$$\tau_{ij}(t+1) = (1-\rho)\,\tau_{ij}(t) - \rho \cdot P_{d_{ij}} \tag{18}$$

where $P_{d_{ij}}$ represents the distance between the last selected sub-region of traversed by the deadlock ant and the flight end point. When the last selected sub-region is farther from flight end point, the attenuation of the pheromone of sub-regions in the sequence is greater. On the contrary, when it is closer to the flight end point, the pheromone of sub-regions traversed are slightly reduced to avoid falling into local optimization.

$$\tau_{ij}(t+1) = (1-\rho)\,\tau_{ij}(t) + \rho\Delta\tau_{ij}(t) \tag{19}$$

$$\Delta\tau_{ij}(t) = Q\left(J_{ij}\right)^{\frac{J_{ij}}{J_{best}}} \tag{20}$$

where J_{best} is the quality evaluation value of the optimal sequence of current iteration. ρ is pheromone volatilization factor.

IV. SIMULATION EXPERIMENT AND ANALYSIS

The applicability of the proposed method is verified by predicting the course of air targets in different scenes. As shown in Fig.8(a), the index values of the course prediction in a simple environment (Scene 1), where the flight airspace is a circle with a radius of 800 km centered on the flight end point. Fig.8(b) shows the attribute values of course

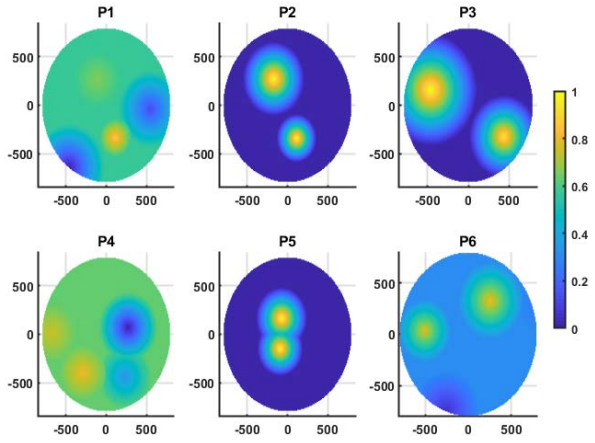

(a) In Scene 1

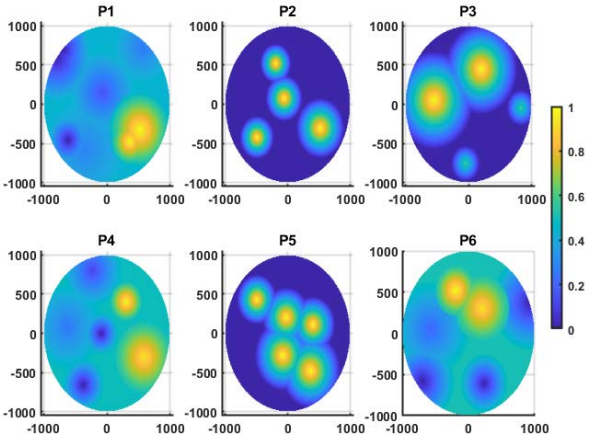

(b) In Scene 2

FIGURE 8. Distributions of course prediction index under different simulation scenes.

prediction indicators in a complex environment (Scene 2), in which the flight airspace is circular with a radius of 1000 km. In this paper, the following points are analyzed separately:

(1) The influence of the weight selection of the quality function J_{course} on the course prediction result is analyzed.
(2) The accuracy and convergence of the course prediction result of different models in scene 1 are analyzed to verify the effectiveness of the proposed method.
(3) In addition, the differences in the course prediction results of different starting points under the same scene are analyzed to verify the robustness of the proposed method.

A. SELECTION OF COURSE QUALITY FUNCTION WEIGHTS

The flight starting point is set to (-518, 612) in scene 1, and combined with the course prediction index, the course of the air target is predicted according to the following three steps.

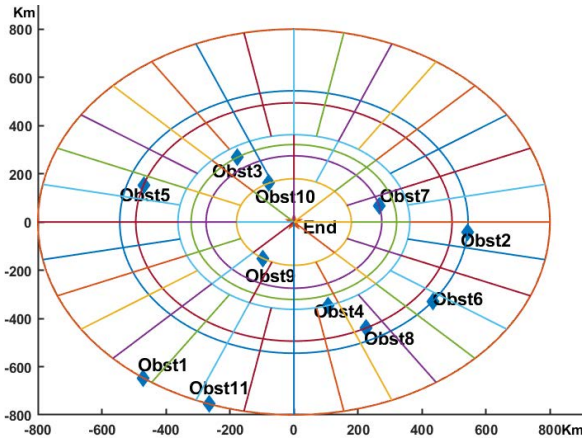

FIGURE 9. Result of adaptive airspace division based on obstacles.

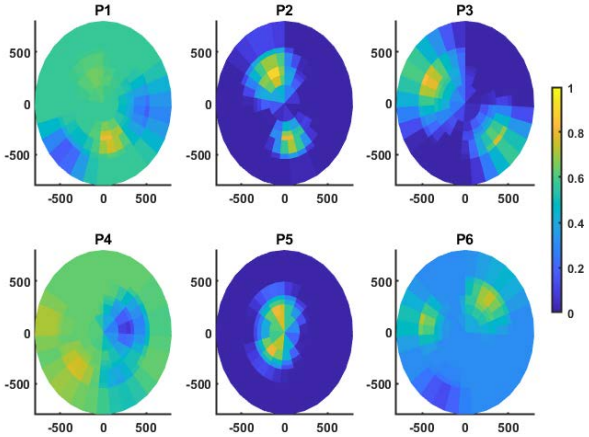

FIGURE 10. Distributions of course prediction indicators in sub-regions based on adaptive decomposition rules.

1) DIVISION RESULTS BASED ON ADAPTIVE DECOMPOSITION RULES

According to the scene information in Fig.8(a), there are 11 flight obstacles in the airspace. In combination with the adaptive decomposition strategy in Section III.B, the flight airspace is divided into 7 ring layers at the first level decomposition rule by taking the distance between the position of each obstacle and the flight destination as the radius. And the corresponding distances are 179.36 km, 274.49 km, 321.03 km, 362.17 km, 493.95 km, 544.06 km, 800 km. Each ring layer is further decomposed according to the second-level decomposition rule, and the airspace division result is shown in Fig.9. And the distributions of 6 indicators in the corresponding sub-regions are shown in Fig.10.

2) CALCULATE THE SELECTION PROBABILITY BASED ON THE BIVARIATE WEIGHT FUNCTION

According to the distributions of course prediction indicators in Fig.10, the weight distribution in each sub-region is calculated based on state variable weight, distance variable weight, and state-distance variable weight. The distance weights of

TABLE 1. The distance weights of sub-regions in different ring layers.

Layers	P1	P2	P3	P4	P5	P6
1	0.1613	0.1722	0.1380	0.1551	0.2423	0.1312
2	0.1653	0.1439	0.2037	0.1579	0.1773	0.1518
3	0.1748	0.1406	0.1922	0.1704	0.1609	0.1611
4	0.1800	0.1391	0.18489	0.1779	0.1508	0.1672
5	0.1871	0.1358	0.1732	0.1913	0.1349	0.1777
6	0.1915	0.1288	0.1655	0.2032	0.1248	0.1863
7	0.2003	0.1149	0.1500	0.2268	0.1046	0.2034

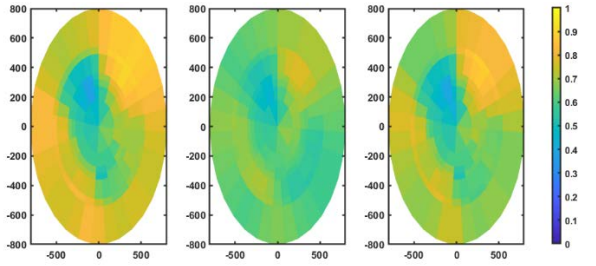

(a) Based on variable weight of index value (b) Based on variable weight of distance (c) Based on bivariate weight

FIGURE 11. Selection possibility distribution of sub-regions with different variable weight functions.

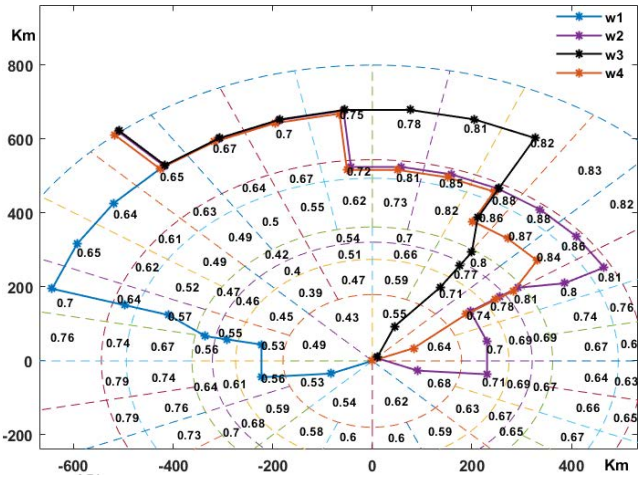

FIGURE 12. Prediction results of different weight of course quality.

the course prediction indicators in different ring layers are shown in Table 1.

The corresponding selection probability distribution results of sub-regions under three different weights are shown in Fig.11. For example, in *7th-6th* layers, the corresponding state values of P_1, P_4, P_6 are low, and the weights of the state value function $S_j(p)$ are in the "punishment" stage, the corresponding state values of P_2, P_3, P_5 are high, and the corresponding weights are in the "incentive" state. Therefore, in Fig.11(a), the selection possibilities of sub-regions in *7th-6th* layers are still relatively high. But when the state value of an indicator is lower than 0.2, the final selection probability is obviously low. The results show that the state variable weight theory can effectively solve the problem of "state imbalance".

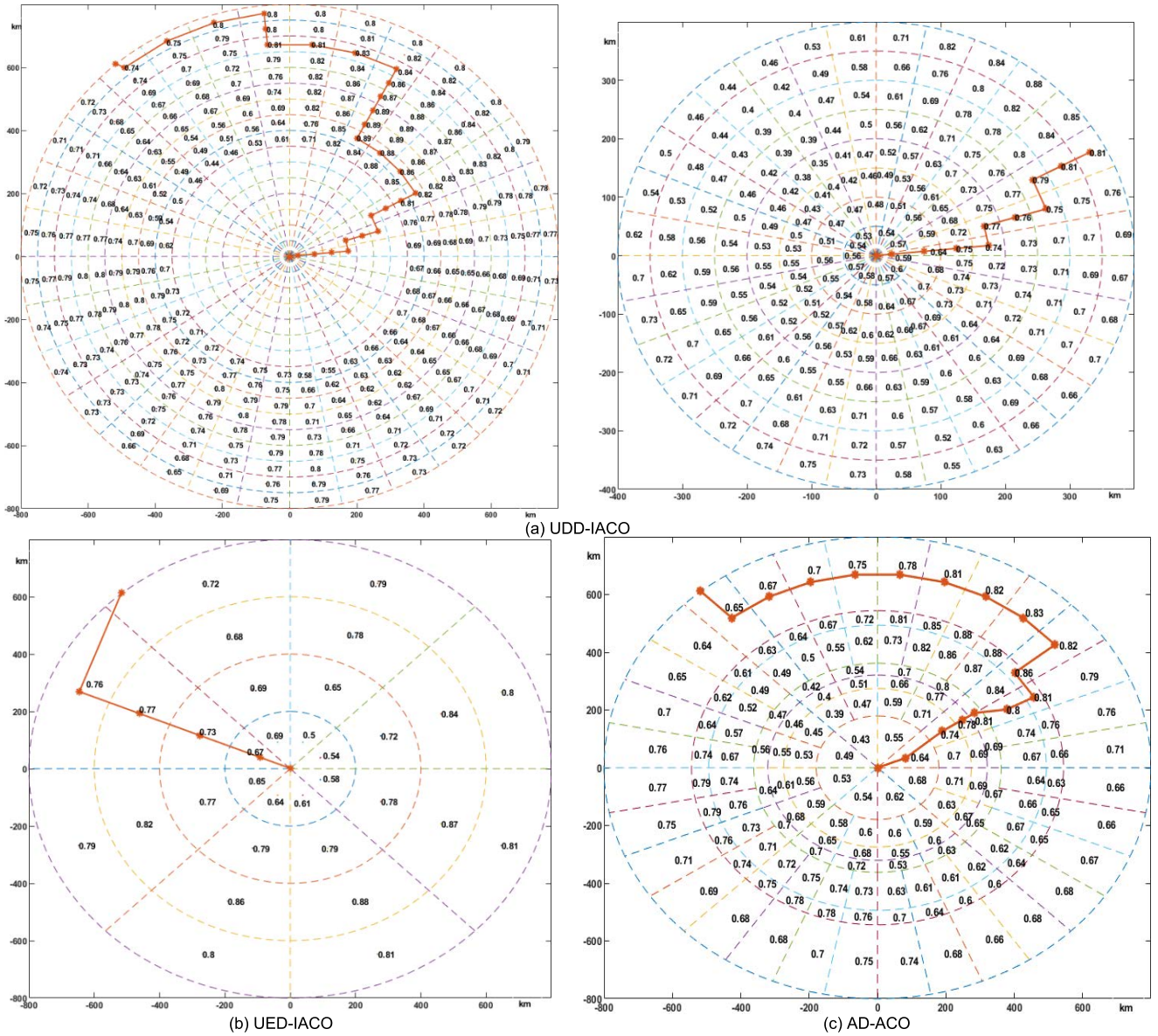

FIGURE 13. Course prediction results based on different models.

According to Table 1, under the influence of the distance variable weight function $S(d)$, the weights of P_1, P_4, P_6 are relatively high, and the corresponding state values of sub-regions in *7th-6th* layers are generally low, so the selection probabilities of sub-regions in *7th-6th* layers in Fig.11(b) are lower than those in Fig.11(a). In the sub-regions of *2nd-1st* layers, the weights of P_2, P_5 are higher, and the selection possibilities of sub-regions are mainly affected by the index P_2, P_5. Therefore, the distance variable weight function $S(d)$ effectively considers the influence of flight distance on the weight of the course index.

Fig.11(c) shows the result of the selection possibility based on state-distance double variable weight. The result integrates the effects of the two variable weights. Compared with Fig.11(b), considering the influence of the index state value on the weight, the degree of ''state imbalance'' is significantly reduced, and the possibility difference values between sub-regions are larger than that in Fig.11(b), which improves the reliability of the sub-region evaluation.

3) SEARCHING FOR A SET OF SUB-REGIONS BASED ON IACO

The search performance of ACO is affected by multiple tightly coupled parameters, and there is a lack of theoretical methods to select the best combination parameter [35]. In this paper, the initial parameters are determined by experience and repeated trial through many experiments [36]. The total number of ants is 50, the maximum number of iterations is set to 100, pheromone importance parameter $\alpha = 2$, heuristic factor importance parameter $\beta = 5$, pheromone evaporation

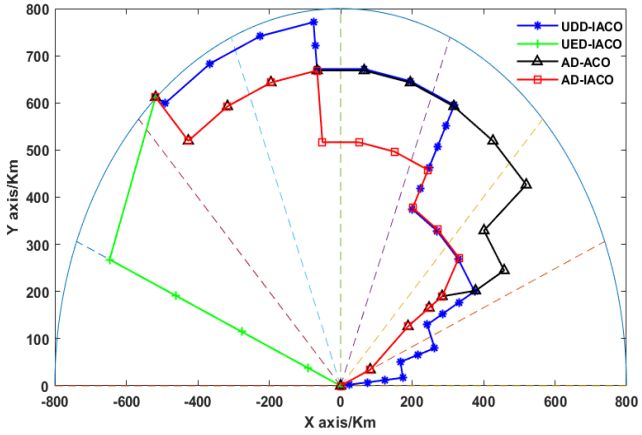

FIGURE 14. Course prediction results in four models.

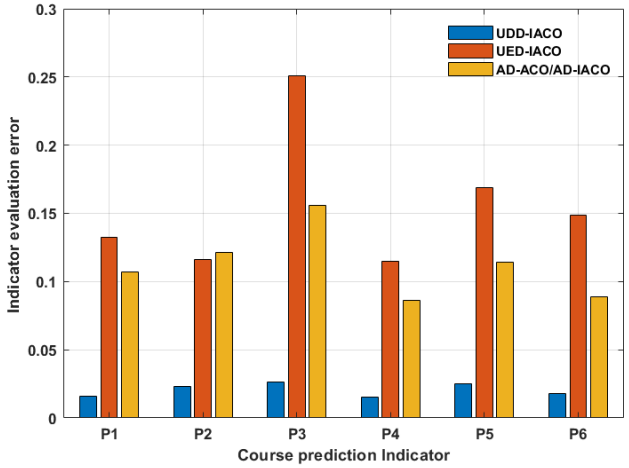

FIGURE 15. Course index evaluation error based on different airspace decomposition rules.

coefficient $\rho = 0.3$ and pheromone increase intensity coefficient $Q = 20$. The influence of the weights in the course sequence quality function Eq.(11) on the flight course prediction result is analyzed and discussed.

Set $[w_{P_L}, w_{P_{cs}}, w_{P_\theta}]$to $w1 = [1, 0, 0]$, $w2 = [0, 1, 0]$, $w3 = [0, 0, 1]$, $w4 = [0.4, 0.3, 0.3]$ respectively, the flight course prediction results in scene 1 are shown in Fig.12.

When the weight $w_{P_{cs}}$ is 1, the sum of the probabilities of predicted course sequence is the largest, and the minimum selection probability of the flying sub-regions is 0.65. In order to make the selected possibility of the course sequence as high as possible, the sequence has the longest length and the highest tortuosity. It can be seen from Fig.12 that when the weight is $w1$, the course sequence is significantly different from the results under other weights. When the weight is $w1$, only the sequence length of sub-regions is considered in course prediction, so the sequence length is the shortest. When the weight is $w3$, the sequence is relatively smooth. However, the sums of sequence possibilities are relatively small under $w1$ and $w3$. According to the Fig.12, the minimum probabilities

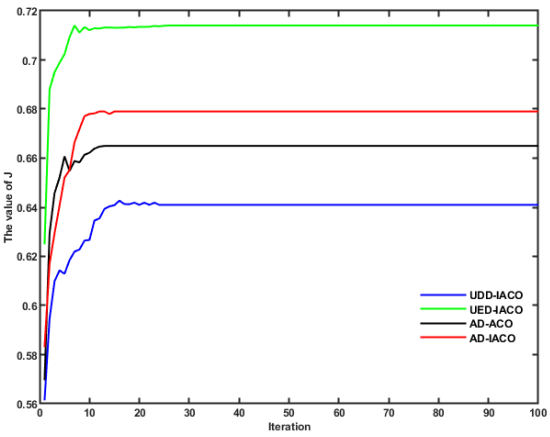

FIGURE 16. Comparison of iterative convergence results.

TABLE 2. Course quality evaluation index in scene 1.

	$W1$	$W2$	$W3$	$W4$
L_{course} / Km	1118.1	1995.7	1603.3	1681.2
CS_{course}	6.58	13.8	9.75	11.57
θ_{course} / π	7.85	16.885	5.10	11.38

of selected sub-regions are 0.53 and 0.55 respectively, which makes it difficult to ensure the flight safety of the target.

When the weight is $w4$, the sum of selection possibilities of sub-region increases by 75.83% and 18.67% respectively compared with $w1$ and $w3$, which effectively improves flight safety. The average probability of sub-regions when the weight is $w4$ is close to that when the weight is $w2$. And according to Fig.12, when the weight is $w4$, the minimum selection probability of the prediction sequence is 0.64. But the sequence length and sequence tortuosity are reduced by 15.76% and 32.6% respectively compared with $w2$.

When the weights are [0.4,0.3,0.3], the result integrates the advantages of three weights. After simulation experiments, when the weight vector is [0.4, 0.3,0.3], the comprehensive evaluation of the course sequence is optimal. Therefore, in this paper, [0.4, 0.3, 0.3] is selected as the final weight of the course sequence quality function.

B. COMPARATIVE ANALYSIS WITH OTHER METHODS

To further verify the accuracy and real-time performance of the proposed method, we analyze the average error between the assessed and real values of the course index *AE,* course sequence quality J and convergence iteration times IT of models. Taking scene 1 as an example, the proposed method (AD-IACO) is compared with the other three models: uniform and dense decomposition-IACO (UDD-IACO), uniform and evacuated decomposition-IACO (UED-IACO), adaptive decomposition-ACO (AD-ACO). The course prediction results of different models in scene 1 are shown in Fig.13. In UDD-IACO, the airspace is uniformly decomposed into different ring layers at intervals of 50 km, and each ring layer

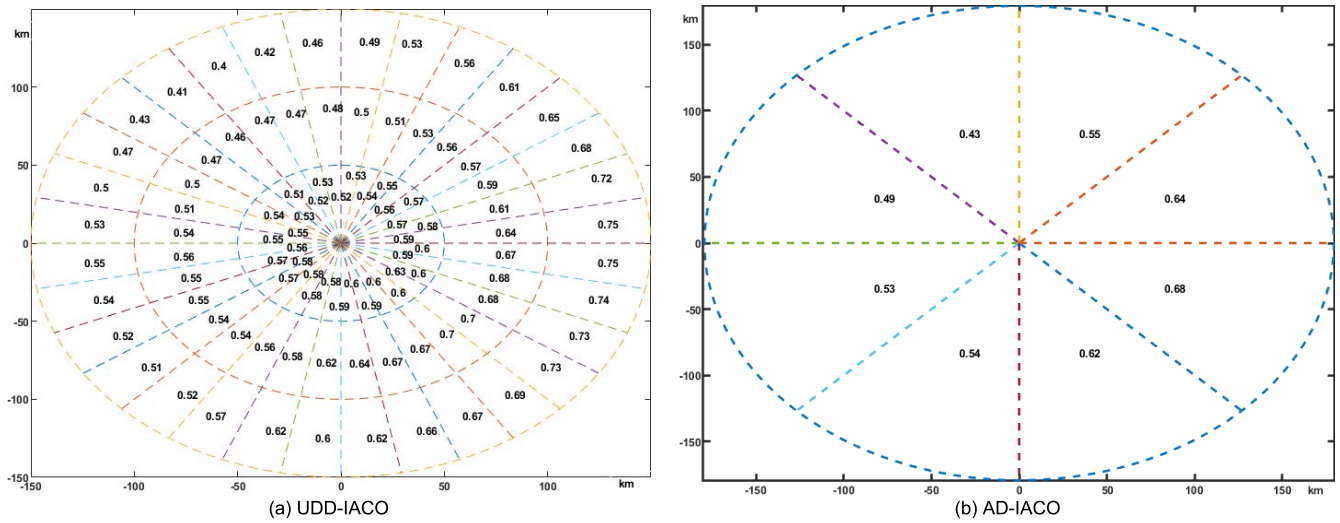

FIGURE 17. Selection probability of sub-region within 150 km in scene 1.

is further decomposed into 32 sub-regions((a)-1 and (a)-2 are the decomposition results of circular airspace within 300-800 km and 0-400 km respectively). In UED-IACO, the airspace is uniformly decomposed at intervals of 200 km, and each ring layer is decomposed into 8 sub-regions. In AD-ACO and AD-IACO, the airspace is adaptively divided according to the distribution of obstruction factors.

It can be seen from Fig.15 that the average error between the assessed value and the real value of the course index in UDD-IACO is the smallest, which is 0.0125. The reliability of the result is the highest. However, according to Fig.16, the initial course quality value J_{course} and the convergence speed are relatively slow. The main reason for this is that UDD-IACO ignores the spatial distribution of obstacles during flight. Taking the airspace of 0-150 km in Scene1 as an example, it is uniformly decomposed into three ring layers in UDD-IACO. There is a slight difference in the selection probabilities between sub-regions of the first ring layer (the probabilities are approximately 0.5). The change trend in selection probability of sub-regions in the 2nd-3rd rings is consistent, and the values are about 0.4-0.7. This shows that the spatial decomposition rule in UDD-IACO increases the number of su-bregions and unnecessarily increases the search space. The first ring layer in AD-IACO is 179.36 km away from the flight destination. Three rings in UDD-IACO are merged into one ring layer, which can reduce the number of sub-regions under the premise of maintaining the consistency of the difference of possibility. Compared with UDD-IACO, the number of iterations is reduced by 41.18%, the convergence speed is greatly improved. In addition, Fig.18 shows the angle change of different course sequences with flight distance. According to Fig.18, it can be seen that the prediction result of AD-IACO is closer to that of UDD-IACO. Therefore, it can be proven that AD-IACO can reduce the number of sub-regions within the range of the index evaluation error and has a faster convergence speed.

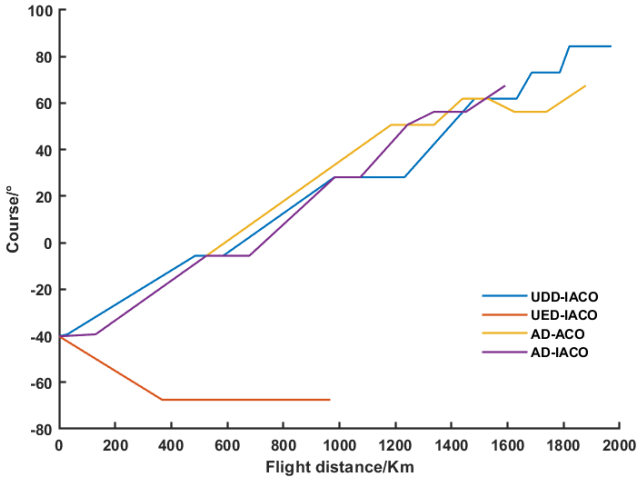

FIGURE 18. Change of course angle in four models.

In UED-IACO, the airspace is uniformly decomposed into evacuated sub-regions. According to the course prediction results of different models in Fig.14, it can be seen that the course prediction results of UED-IACO are quite different from those of other models. Combined with the data in Fig.15, it can be seen that the average evaluation error of course prediction index in UED-IACO is relatively large, especially the average error of P_3 is 0.2084. Although Fig.16 shows that the course prediction quality and convergence speed are good, the reliability of the results is extremely low. UED-IACO cannot provide a basis for decision support. Although the quality of the course sequence of AD-IACO is reduced by 4.77% and the number of iterations is increased by 42.86% owing to the more complex spatial decomposition results, the average evaluation error of course prediction index is reduced by 58.47%, which makes the results more reliable.

The errors of course prediction indicators in AD-ACO are consistent with those in AD-IACO because of the adaptive

TABLE 3. Comparison of course prediction results in scene 1.

	UDD-IACO	UED-IACO	AD-ACO	AD-IACO
AE	0.0125	0.1269	0.0524	0.0524
IT	17	7	12	10
J	0.641	0.713	0.665	0.679

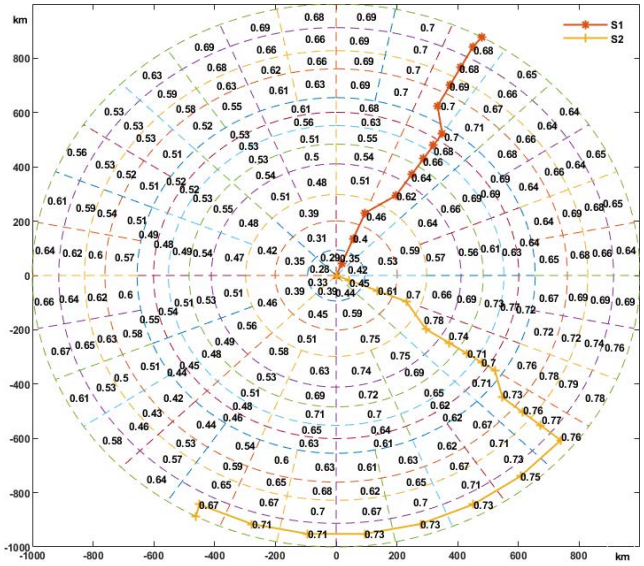

FIGURE 19. Course prediction results in scene 2 based on AD-IACO.

spatial decomposition rules, but the former has a slightly lower convergence quality than the latter. In particular, the former has a slower convergence speed. On the one hand, the heuristic function of AD-ACO only considers the selection possibility of sub-regions when searching for a set of sub-regions, which leads to that the target cannot approach the destination in time, so its course sequence length is long, and the course convergence quality is low. On the other hand, AD-ACO uses global pheromone update rule, which takes a long time to play the role of positive feedback, resulting in a slow convergence speed. According to the results in Table 3, compared with AD-ACO, the number of convergence iterations of AD-IACO has decreased by 16.67%, which indicates that it is effective to construct heuristic functions based on distance factor and possibility factor and pheromone update rules based on positive and negative feedback.

Based on the above analysis, the adaptive decomposition rules can improve the convergence quality and convergence speed of course prediction on the premise of ensuring the reliability of the prediction results. In addition, the heuristic function and pheromone updating rules of ACO are improved, which effectively solves the disadvantage of the slow convergence speed of ACO and improves the real-time performance of course prediction.

C. ROBUSTNESS ANALYSIS

To verify the robustness of the proposed AD-IACO model, the flight starting points are set as Situation 1(S1) and Situation 2(S2) respectively in scene 2. The corresponding target

TABLE 4. Course sequence evaluation index in scene 2.

	S1	S2
L_{course} / Km	1476.0	1808.6
CS_{course}	9.17	15.38
θ_{course} / π	7.67	12.91

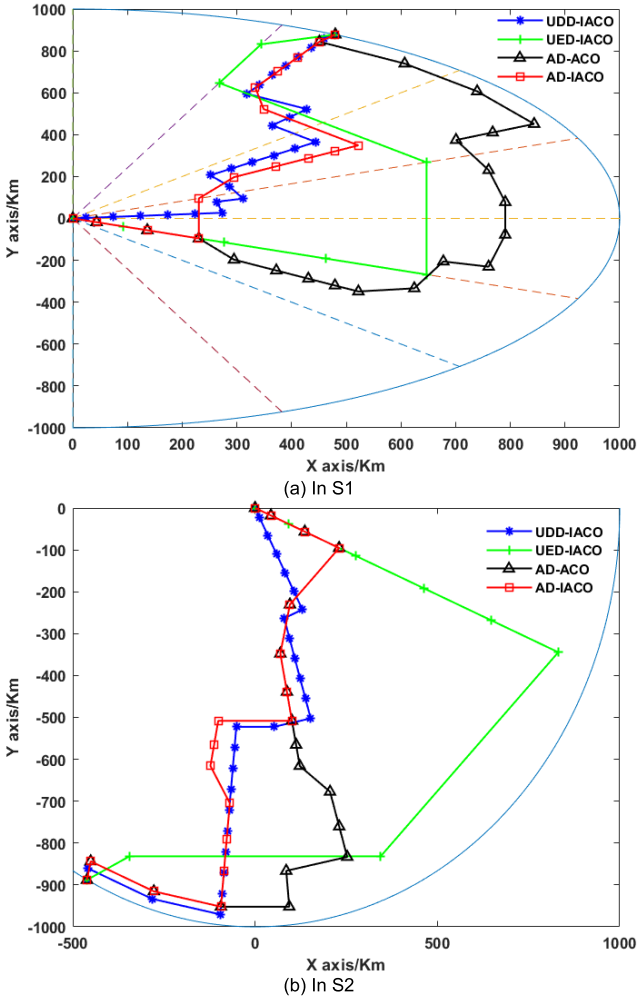

FIGURE 20. Course prediction results based on different models in scene 2.

starting points are (480 km,870 km) and (−461 km, −888 km) respectively. The predicted course sequences are shown in Fig.19, and the corresponding course quality evaluation indicators are shown in Table 4. As shown, compared with the course prediction results in scene 1, the length and tortuosity of the course sequence are relatively large in scene 2.

Similarly, we compare the course prediction results of different models under the two situations in scene 2. According to Fig.20, it can be seen that the course prediction results of the models are more consistent. But combining the convergence results of different models in Fig.21, the course prediction results of AD-IACO still have high course quality values and fast convergence speeds.

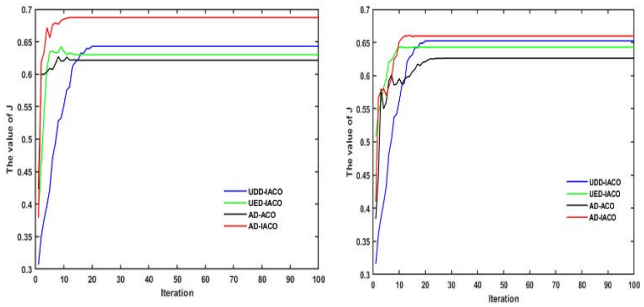

FIGURE 21. Iterative convergence results based on different models in scene2.

TABLE 5. Comparison of course prediction results in scene 2.

	AE	*IT*		*J*	
		S1	S2	S1	S2
UDD-IACO	0.0206	21	20	0.643	0.652
UED-IACO	0.2553	12	11	0.630	0.643
AD-ACO	0.1323	14	23	0.621	0.652
AD-IACO	0.1323	12	15	0.687	0.659

It can be seen from Table 5, UED-IACO has a large error in course prediction indicators compared with other models, so the reliability of prediction results based on indicator status values is low. The error of AD-IACO is reduced by 0.123 compared with UED-IACO. At the same time, the numbers of iterations are the same as those in UED-IACO. In addition, compared with UDD-IACO and AD-ACO, the numbers of convergence iterations of AD-IACO in scene 2 are significantly reduced. Especially in S2, the number of iterations is reduced by 25% and 34.78% respectively. The convergent course qualities of AD-IACO are the highest in S1 and S2.

The results show that in complex situations such as scene 2, the performance of AD-IACO model still takes into account the reliability and real-time performance of course prediction results, and the course prediction results at different starting points of the path verify the robustness of the model.

V. CONCLUSION

In this paper, an air target course prediction method based on sub-regions divide and conquer with double variable weight is proposed and verified in different simulation environments. The simulation results show that the adaptive decomposition of airspace based on obstacle factors can reduce the number of sub-region and improve the search efficiency of sub-regions on the premise of ensuring the reliability of course prediction. In addition, compared with ACO, the improved ant colony algorithm is used to predict the course sequence of air targets, and the course convergence speed is increased by 34.78% on average.

The simulation results show that the proposed method can take into account the accuracy and real-time of course prediction, which is of great significance to the deployment decision. In this study, the global course prediction method based on macro modal constraints is studied. In the future, the local 3D trajectory of air targets will be further studied based on the global course sequence in combination with the motion performance constraints of air targets.

REFERENCES

[1] E. Sepulveda and H. Smith, "Technology challenges of stealth unmanned combat aerial vehicles," *Aeronaut. J.*, vol. 121, no. 1243, pp. 1261–1295, Sep. 2017.

[2] J. Qin and X. Wu, "Modeling and simulation on the earliest launch time of ship-to-air missile of warship formation in cooperative air-defense," in *Proc. IEEE Adv. Inf. Manage., Communicates, Electron. Autom. Control Conf. (IMCEC)*, Xi'an, China, Oct. 2016, pp. 375–379, doi: 10.1109/IMCEC.2016.7867237.

[3] Y. Gao, D. Li, and H. Zhong, "A novel target threat assessment method based on three-way decisions under intuitionistic fuzzy multi-attribute decision making environment," *Eng. Appl. Artif. Intell.*, vol. 87, Jan. 2020, Art. no. 103276, doi: 10.1016/j.engappai.2019.103276.

[4] M. R. Endsley, "Toward a theory of situation awareness in dynamic systems," *Hum. Factors, J. Hum. Factors Ergonom. Soc.*, vol. 37, no. 1, pp. 32–64, Mar. 1995, doi: 10.1518/001872095779049543.

[5] J. Song and H. Xu, "Fuzzy forecast method of the main direction of attack in the coastal defense battle," *Comput. Digit. Eng.*, vol. 42, no. 1, pp. 19–21, Jan. 2014.

[6] D. Ren and Z. Cao, "Judging main orientation of enemy air attack based on grey hierarchical theory," *Comput. Sci.*, vol. 36, no. 1, pp. 208–210, Jan. 2009.

[7] A. M. Zhu, F. W. Zhang, W. F. Shen, and H. Y. Yu, "Study on main attacking direction of enemy's air raid weapons based on FCE," *J. Sichuan Ordnance*, vol. 36, no. 7, pp. 21–23, Jul. 2015.

[8] L. Ji, F. Yang, and X. Wang, "A possibility estimation model and its application in adhesive structure," *Appl. Mech. Mater.*, vols. 457–475, no. 6, pp. 423–427, Dec. 2013, doi: 10.4028/www.scientific.net/AMM.475-476.423.

[9] S. Ge and X. Xia, "DSBN used for recognition of tactical intention," *Syst. Eng. Electron.*, vol. 36, no. 1, pp. 77–83, Oct. 2014.

[10] J. Qian, X. Jin, S. Lee, and S. Yao, "A new similarity/distance measure between intuitionistic fuzzy sets based on the transformed isosceles triangles and its applications to pattern recognition," *Exp. Syst. Appl.*, vol. 116, pp. 439–453, Aug. 2018, doi: 10.1016/j.eswa.2018.08.046.

[11] F. B. Yang, L. N. Ji, and X. X. Wang, "Decision making method based on possibility theory," in *Possibility Theory and Applications*, 1st ed. Beijing, China: Science Press, 2019, ch.7, sec. 2, pp. 133–140.

[12] T. Yang, Y. Wang, and B. Tan, "Application of multi-index optimization method in determining primary air attack direction of enemy," *Ship Electron. Eng.*, vol. 30, no. 4, pp. 50–52, Apr. 2010.

[13] X. Ma, K. Teng, and X. Hou, "Convolutional neural network judgment model for main attack direction of air raid," *Modern Defense Technol.*, vol. 46, no. 5, pp. 6–12, Oct. 2018.

[14] C. Zhou, S. Gu, Y. Wen, Z. Du, C. Xiao, L. Huang, and M. Zhu, "The review unmanned surface vehicle path planning: Based on multi-modality constraint," *Ocean Eng.*, vol. 200, Mar. 2020, Art. no. 107043, doi: 10.1016/j.oceaneng.2020.107043.

[15] J.-M. Yang, C.-M. Tseng, and P. S. Tseng, "Path planning on satellite images for unmanned surface vehicles," *Int. J. Nav. Archit. Ocean Eng.*, vol. 7, no. 1, pp. 87–99, Jan. 2015, doi: 10.1515/ijnaoe-2015-0007.

[16] R. Song, Y. Liu, and R. Bucknall, "Smoothed A* algorithm for practical unmanned surface vehicle path planning," *Appl. Oceans Res.*, vol. 83, pp. 9–20, Feb. 2019, doi: 10.1016/j.apor.2018.12.001.

[17] L. Chong, L. Jian, and L. XueQuan, "Static rectangle expansion A* algorithm for pathfinding," *IEEE Trans. Games*, vol. 14, no. 1, pp. 23–35, Mar. 2022, doi: 10.1109/TG.2020.3012602.

[18] Z. Ren, S. Rathinam, and H. Choset, "Multi-objective path-based D* lite," *IEEE Robot. Autom. Lett.*, vol. 7, no. 2, pp. 3318–3325, Apr. 2021, doi: 10.48550/arXiv.2108.00710.

[19] C. Miao, G. Chen, C. Yan, and Y. Wu, "Path planning optimization of indoor mobile robot based on adaptive ant colony algorithm," *Comput. Ind. Eng.*, vol. 156, Jun. 2021, Art. no. 107230, doi: 10.1016/j.cie.2021.107230.

[20] R. Zheng, Y. Zhang, and K. Yang, "A transfer learning-based particle swarm optimization algorithm for travelling salesman problem," *J. Comput. Des. Eng.*, vol. 9, no. 3, pp. 933–948, May 2022, doi: 10.1093/jcde/qwac039.
[21] M. A. Alanezi, H. R. E. H. Bouchekara, T. A.-A. Apalara, M. S. Shahriar, Y. A. Sha'aban, M. S. Javaid, and M. A. Khodja, "Dynamic target search using multi-UAVs based on motion-encoded genetic algorithm with multiple parents," *IEEE Access*, vol. 10, pp. 77922–77939, 2022, doi: 10.1109/ACCESS.2022.3190395.
[22] P. Yao, Q. Zhu, and R. Zhao, "Gaussian mixture model and self-organizing map neural-network-based coverage for target search in curve-shape area," *IEEE Trans. Cybern.*, vol. 52, no. 5, pp. 3971–3983, May 2022, doi: 10.1109/TCYB.2020.3019255.
[23] L. Zhai and S. Feng, "An improved ant colony algorithm based on artificial potential field and quantum evolution theory," *J. Intell. Fuzzy Syst.*, vol. 42, no. 6, pp. 5773–5788, Apr. 2022, doi: 10.3233/JIFS-212220.
[24] R. An, S. Guo, L. Zheng, H. Hirata, and S. Gu, "Uncertain moving obstacles avoiding method in 3D arbitrary path planning for a spherical underwater robot," *Robot. Auto. Syst.*, vol. 151, May 2022, Art. no. 104011, doi: 10.1016/j.robot.2021.104011.
[25] Z.-M. Huang, W.-N. Chen, Q. Li, X.-N. Luo, H.-Q. Yuan, and J. Zhang, "Ant colony evacuation planner: An ant colony system with incremental flow assignment for multipath crowd evacuation," *IEEE Trans. Cybern.*, vol. 51, no. 11, pp. 5559–5572, Nov. 2021, doi: 10.1109/TCYB.2020.3013271.
[26] T. Xue, L. Li, L. Shuang, D. Zhiping, and P. Ming, "Path planning of mobile robot based on improved ant colony algorithm for logistics," *Math. Biosci. Eng.*, vol. 18, no. 4, pp. 3034–3045. Mar. 2021, doi: 10.3934/mbe.2021152.
[27] Z. Lin, Z. Chen, J. Liu, and Q. Wu, "Coordinated mechanical loads and power optimization of wind energy conversion systems with variable-weight model predictive control strategy," *Appl. Energy*, vol. 236, pp. 307–317, Feb. 2019, doi: 10.1016/j.apenergy.2018.11.089.
[28] C. Lin, M. Zhang, Z. Zhou, L. Li, S. Shi, Y. Chen, and W. Dai, "A new quantitative method for risk assessment of water inrush in Karst tunnels based on variable weight function and improved cloud model," *Tunnelling Underground Space Technol.*, vol. 95, Jan. 2020, Art. no. 103136, doi: 10.1016/j.tust.2019.103136.
[29] T. Zhang, G. Chen, Q. Zeng, G. Song, C. Li, and H. Duan, "Routing clustering protocol for 3D wireless sensor networks based on fragile collection ant colony algorithm," *IEEE Access*, vol. 8, pp. 58874–58888, 2020, doi: 10.1109/ACCESS.2020.2982691.
[30] S. Ye and Z. Wan, "An ant colony algorithm based on improved global pheromone updating efficiency and its simulation," *Comput. Appl. Softw.*, vol. 31, no. 1, pp. 176–179, Jan. 2014.
[31] Z. Chen and X. Han, "Application of improved ant colony algorithm in mobile robot path planning," *Comput. Eng. Des.*, vol. 41, no. 8, pp. 2388–2395, Aug. 2020.
[32] F. Hu and G. Wang, "Knowledge reduction based on divide and conquer method in rough set theory," *Math. Problems Eng.*, vol. 2012, pp. 1–24, Jan. 2012, doi: 10.1155/2012/864652.
[33] X. Li, L. Li-jia, J. Yan, and L. Rui, "Air attack weapons attacking direction prejudgment before the deployment of anti-air weapons for the key point," *Syst. Eng.-Theory Pract.*, vol. 34, no. 35, pp. 1330–1338, May 2014.
[34] R. Huang, J. Ning, Z. Mei, X. Fang, X. Yi, Y. Gao, and G. Hui, "Study of delivery path optimization solution based on improved ant colony model," *Multimedia Tools Appl.*, vol. 80, no. 19, pp. 28975–28987, Aug. 2021, doi: 10.1007/s11042-021-11142-1.
[35] B. Erin, R. Abiyev, and D. Ibrahim, "Teaching robot navigation in the presence of obstacles using a computer simulation program," *Proc. Social Behav. Sci.*, vol. 2, no. 2, pp. 565–571, 2010, doi: 10.1016/j.sbspro.2010.03.064.
[36] J. Liu, Y. Jianguo, L. Huaping, G. Peng, and G. Meng, "Robot global path planning based on ant colony optimization with artificial potential field," *Trans. Chin. Soc. Agricult. Machinery*, vol. 46, no. 9, pp. 18–27, May 2015.

TONGYAO YANG was born in Shanxi, China, in 1997. She received the B.Eng. degree from the Fujian University of Technology, China, in 2019. She is currently pursuing the Ph.D. degree in communication and information engineering with the North University of China, China. Her current research interest includes situation prediction.

FENGBAO YANG received the Ph.D. degree in measurement technology and instrument from the North University of China, Taiyuan, China, in 2003. From 2004 to 2007, he was a Postdoctoral Research Fellow with the Beijing Institute of Technology. Currently, he is a Full Professor with the North University of China. His current research interests include information fusion and information fusion theory of uncertainty. He has presided over three items of the National Natural Science Foundation. He has published approximately 100 papers in the information fusion and image processing journals and eight books on uncertain information reasoning methods and infrared technology.

DINGZHU LI is currently a Senior Engineer at the North Automatic Control Technology Institute. His current research interests include automatic control, network information, and numerical simulation. His honors include the second prize of the National Science and Technology Progress Award, the Provincial and Ministerial Science, and Technology Progress Special Award.